

Multi-Hypothesis Pose Networks: Rethinking Top-Down Pose Estimation

Rawal Khirodkar^{1*}

Visesh Chari²

Amit Agrawal²

Amrisha Tyagi²

¹Carnegie Mellon University

²Amazon Lab 126

rkhirod@cs.cmu.edu

{viseshc, aaagrawa, ambrisht}@amazon.com

Abstract

A key assumption of top-down human pose estimation approaches is their expectation of having a single person present in the input bounding box. This often leads to failures in crowded scenes with occlusions. We propose a novel solution to overcome the limitations of this fundamental assumption. Our Multi-Hypothesis Pose Network (MHPNet) allows for predicting multiple 2D poses within a given bounding box. We introduce a Multi-Hypothesis Attention Block (MHAB) that can adaptively modulate channel-wise feature responses for each hypothesis and is parameter efficient. We demonstrate the efficacy of our approach by evaluating on COCO, CrowdPose and OCHuman datasets. Specifically, we achieve 70.0 AP on CrowdPose and 42.5 AP on OCHuman test sets, a significant improvement of 2.4 AP and 6.5 AP over prior art, respectively. When using ground truth bounding boxes for inference, MHPNet achieves an improvement of 0.7 AP on COCO, 0.9 AP on CrowdPose, and 9.1 AP on OCHuman validation sets compared to HRNet. Interestingly, when fewer, high confidence bounding boxes are used, HRNet's performance degrades (by 5 AP) on OCHuman, whereas MHPNet maintains a relatively stable performance (drop of 1 AP) for the same inputs.

1. Introduction

Human pose estimation aims at localizing 2D human anatomical keypoints (e.g., elbow, wrist, etc.) in a given image. Current human pose estimation methods can be categorized as *top-down* or *bottom-up* methods. Top-down methods [5, 11, 30, 36, 37, 38, 39] take as input an image region within a bounding box, generally the output of a human detector, and reduce the problem to the simpler task of *single human pose estimation*. Bottom-up methods [3, 19, 27, 29], in contrast, start by independently localizing keypoints in the entire image, followed by grouping them into 2D human pose instances.



Figure 1: 2D pose estimation networks often fail in presence of heavy occlusion. (Left) Bounding boxes corresponding to two persons. (Middle) For both bounding boxes, HRNet predicts the pose for the front person and misses the occluded person. (Right) MHPNet allows multiple hypotheses for each bounding box and recovers the pose of the occluded person.

The single human assumption made by top-down approaches limits the inference to a *single* configuration of human joints that can best explain the input. Top-down pose estimation approaches [5, 13, 28, 36, 39] are currently the best performers on datasets such as COCO [22]. However, when presented with inputs containing multiple humans like crowded or occluded instances, top-down methods are forced to select a single plausible configuration per human detection. In such cases, top-down methods may erroneously identify pose landmarks corresponding to the occluder (person in the front). See, for example, Fig. 1 (Middle). Therefore, on datasets such as CrowdPose [20] and OCHuman [43], which

*Work done during an internship at Amazon Lab 126

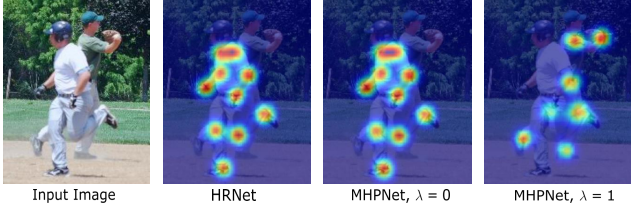


Figure 2: Heatmap predictions for a few keypoints from HRNet vs MHPNet. HRNet outputs a single pose prediction and focuses on the foreground person. MHPNet enables prediction of the multiple hypotheses from the *same* input bounding box by varying λ during inference.

have a relatively higher proportion of occluded instances (Table 1), the performance of top-down methods suffer due to the single person assumption [7, 20, 43].

In this paper, we rethink the architecture for top-down 2D pose estimators by allowing for *multiple* pose hypotheses for the input bounding box. The key idea of our proposed Multi-Hypothesis Pose Network (MHPNet) architecture is to allow the model to predict more than one pose instance for each bounding box. We demonstrate that this conceptual change improves the performance of top-down methods, especially for instances with crowding and heavy occlusion. A naïve approach to predict multiple poses per bounding box would be to add multiple prediction heads to an existing top-down network with a shared feature-extraction backbone. However, such an approach fails to learn different features corresponding to the various hypotheses. A brute-force approach would then be to replicate the feature-extraction backbone, though at a cost of an N -fold increase in parameters, for N hypotheses. In contrast, our approach enables predicting multiple hypotheses for any existing top-down architecture with a small increase in the number of parameters ($< 3\%$), independent of N .

To enable efficient training and inference of multiple pose hypotheses in a given bounding box, we propose a novel Multi-Hypothesis Attention Block (MHAB). MHAB modulates the feature tensors based on a scalar parameter, λ , and allows MHPNet to index on one of the N hypotheses (Fig. 2). MHAB can be incorporated in any existing feature-extraction backbone, with a relatively simple (< 15 lines) code change (see supplementary materials). At inference, for a given bounding box, we vary λ to generate different pose predictions (Fig. 3).

Since top-down approaches rely on the output from an object detector, they typically process a large number of bounding box hypotheses. For example, HRNet [36] uses more than 100K bounding boxes from Faster R-CNN [34] to predict 2D pose for ~ 6000 persons in the COCO val dataset. Many of these bounding boxes overlap and majority have low detection scores (< 0.4). This also adversely impacts the inference time, which increases linearly with

Dataset	IoU > 0.5	ΔAP_0	$\Delta AP_{0.9}$	ΔAP_{gt}
COCO	1.2K (1%)	0.0	+1.9	+0.7
CrowdPose	2.9K (15%)	+0.8	+2.3	+0.9
OCHuman	3.2K (68%)	+4.2	+8.2	+9.1

Table 1: MHPNet’s relative improvement in AP compared to HRNet-W48 on the val set, using Faster R-CNN (AP_0 : all, $AP_{0.9}$: high confidence) and ground truth (AP_{gt}) bounding boxes. For each dataset, the number (%) of instances with occlusion IoU > 0.5 is reported [32]. Datasets with more occlusions and crowding demonstrate higher gains.

the number of input bounding boxes. As shown in Fig. 4, using fewer, high confidence bounding boxes degrades the performance of HRNet from 37.8 to 32.8 AP on OCHuman, a degradation of 5 AP in performance. In contrast, MHPNet is robust and maintains a relatively stable performance for the same inputs (drop of 1 AP). Intuitively, our method can predict the 2D pose corresponding to a mis-detected bounding box based on predictions from its neighbors.

Overall, MHPNet outperforms top-down methods (*e.g.* HRNet, SimpleBaseline [39]) on various datasets as shown in Table 1. For challenging datasets such as CrowdPose and OCHuman, containing a larger proportion of cluttered scenes (with multiple overlapping people), MHPNet sets a new state-of-the-art achieving 70.0 AP and 42.5 AP respectively on the test set outperforming bottom-up methods. Our main contributions are

- We advance top-down 2D pose estimation methods by addressing limitations caused by the single person assumption during training and inference. Our approach achieves the state-of-the-art results on CrowdPose and OCHuman datasets.
- MHPNet allows predicting multiple hypotheses for a given bounding box efficiently by introducing a novel attention mechanism, MHAB. MHAB can modulate feature responses in a network for each hypothesis independently.
- The ability to predict multiple hypotheses makes MHPNet resilient to bounding box confidence and allows it to deal with missing bounding boxes with minimal impact on performance.

2. Related Work

Biased benchmarks: Most human pose estimation benchmarks [1, 2, 10, 17, 22] do not uniformly represent possible poses and occlusions in the real world. Popular datasets such as COCO [22] and MPII [2] have less than 3% annotations with crowding at IoU of 0.3 [32]. More than 86% of annotations in COCO [22] have 5 or more keypoints

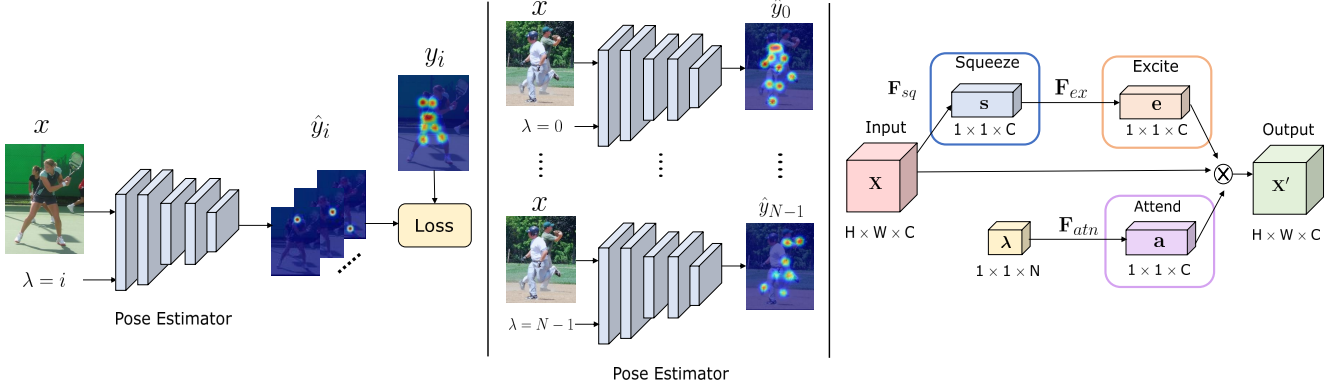


Figure 3: (Left) MHPNet is trained to predict the i^{th} hypothesis from an input x by conditioning the network using $\lambda = i$, $\forall i = 0, \dots, N - 1$. (Middle) During inference, we obtain the N pose predictions by varying λ . (Right) MHAB uses squeeze, excitation and attention modules that enables λ to modulate the feature responses for each hypothesis.

visible [35]. These biases have seeped into our state-of-the-art data driven deep learning models [40], not only in the form of poor generalization to “in-the-tail” data but surprisingly in critical design decisions for network architectures. Recently, challenging datasets such as OCHuman [43] and CrowdPose [20] containing heavy occlusion and crowding have been proposed to capture these biases. These datasets demonstrate the failures of the state-of-art models under severe occlusions (Section 4.3). Our approach shows a significant improvement in performance under such challenging conditions.

Top-down methods: Top-down methods [5, 9, 11, 13, 28, 30, 36, 39] detect the keypoints of a single person within a bounding box. These bounding boxes are usually generated by an object detector [6, 21, 23, 33, 34]. As top-down methods can normalize all the persons to approximately the same scale by cropping and resizing the detected bounding boxes, they are generally less sensitive to scale variations in images. Thus, state-of-the-art performances on various human pose estimation benchmarks are mostly achieved by top-down methods [36]. However, these methods inherently assume a single person in the detection window and often fail under occlusions. Since top-down methods are gated by person detection, these methods fail to recover an instance if it is missing in detection results. Since our approach allows multiple hypothesis for each detection, it could recover some of these instances if they are present within the bounding box of a *different* person, even-though such instances themselves may be missing from bounding box detection.

Bottom-up methods: Bottom-up methods [3, 7, 14, 15, 27, 31] detect identity-free instance agnostic body joints for all the persons in an image and then group them into full-body keypoints. This enables bottom-up methods to be faster and more capable of achieving real-time pose estimation. However, the grouping methods often employ various heuristics and require hyper-parameter tuning. Furthermore,

due to identity-free detection, bottom-up methods are robust to occlusion [7, 43] and better capable in handling complex poses. However, because bottom-up methods need to deal with scale variation, they perform poorly on small scale persons in comparison to top-down methods [7, 36].

Multi-Hypothesis Learning: In machine learning, many models have been trained to behave differently depending on a conditional input [4, 8, 18, 24, 25, 41]. In multi-task networks, separate models with different weighing of loss terms are often trained to obtain multiple solutions. Instead of training multiple models, our approach enables training a single network for predicting multiple hypothesis on the same input. Instead of duplicating the feature backbone, our novel MHAB block leads to a parameter efficient design.

3. Method

Human pose estimation aims to detect the locations of K keypoints from an input image $x \in \mathbb{R}^{H \times W \times 3}$. Most top-down methods transform this problem to estimating K heatmaps, where each heatmap indicates the probability of the corresponding keypoint at any spatial location. Similar to [5, 28, 39] we define a convolutional pose estimator, P , for human keypoint detection. The bounding box at training and inference is scaled to $H \times W$ and is provided as an input to P . Let $y \in \mathbb{R}^{H' \times W' \times K}$ denote the K heatmaps corresponding to the ground truth keypoints for a given input x . The pose estimator transforms input x to a single set of predicted heatmaps, $\hat{y} \in \mathbb{R}^{H' \times W' \times K}$, such that $\hat{y} = P(x)$. P is trained to minimize the mean squared loss $\mathcal{L} = \text{MSE}(y, \hat{y})$.

3.1. Multi-Hypothesis Learning

We propose to modify the top-down pose estimator P to predict multiple hypotheses as follows. Our pose estimator P predicts N hypotheses, $\hat{y}_0, \dots, \hat{y}_{N-1}$ for input x . This is achieved by conditioning the network P on a scalar λ , $0 \leq \lambda \leq N - 1$. P accepts both x and λ as input and

predicts $\hat{y}_i = P(x, \lambda = i)$, where $i \in \{0, 1, \dots, N - 1\}$.

Let B_0 denote the ground truth bounding box used to crop the input x . Let $B_i, i \in \{1, \dots, n - 1\}$, denote additional $n - 1$ ground truth bounding boxes which overlap B_0 , such that at least $k = 3$ keypoints from B_i fall within B_0 . Thus, B_0, \dots, B_{n-1} represents the bounding boxes for n ground truth pose instances present in x . We denote the ground truth heatmaps corresponding to these n instances by y_0, \dots, y_{n-1} .

To define a loss, we need to assign the predicted pose hypotheses to the ground truth heatmaps. The primary hypothesis $\hat{y}_0 = P(x, \lambda = 0)$ is assigned to y_0 , the pose instance corresponding to B_0 . The next $n - 1$ hypotheses are assigned to the remaining ground truth heatmaps ordered according to the distance of their corresponding bounding box from B_0 . We train the network P to minimize the loss $\mathcal{L} = \frac{1}{N} \sum_{i=0}^{N-1} \mathcal{L}_i$, where,

$$\mathcal{L}_i = \begin{cases} \text{MSE}(y_i, P(x, \lambda = i)), & \forall 0 \leq i < n, \\ \text{MSE}(y_0, P(x, \lambda = i)), & \forall n \leq i < N. \end{cases} \quad (1)$$

Equation 1 uses n hypotheses to compute the loss with respect to the n ground truth pose instances, y_0, \dots, y_{n-1} . It also computes the loss for the *residual* $N - n$ hypotheses using y_0 . For example, when $n = 1$ and $N = 2$, both the predictions are encouraged to predict the heatmaps corresponding to the single ground truth instance present in x .

In our experience, employing other heuristics such as not propagating the loss, *i.e.*, *don't care* for residual hypotheses resulted in less stable training. Additionally, a *don't care* based training scheme for residual hypotheses resulted in significantly higher false positives, especially as we do not know the number of valid person instances per input at runtime. During inference, we vary λ to extract different pose predictions from the same input x as shown in Fig. 3.

3.2. Multi-Hypothesis Attention Block

In this section, we describe our Multi-hypothesis Attention Block (MHAB) that can be easily introduced in any existing feature extraction backbone used for human pose estimation. MHAB allows top-down pose estimator P to accept both x and λ as inputs and builds upon the squeeze excitation block of [12]. Let $\mathbf{X} \in \mathbb{R}^{P \times Q \times C}$ be an intermediate feature map with C channels, such that $\mathbf{X} = [\mathbf{x}_1, \mathbf{x}_2, \dots, \mathbf{x}_C]$. We introduce attention through λ by modulating the channel wise activations of the output of the excitation block as shown in Fig. 3 (Right).

The key insight of our design is that we can use the same set of convolutional filters to dynamically attend to different hypotheses corresponding to the multiple pose instances in the input. Compared to a brute force approach of replicating the feature backbone or assigning a fixed number of channels per hypothesis, our design is parameter efficient. MHAB allows for channel-wise information exchange through the

squeeze and excitation process inherent in the block. Combining squeeze and excitation modules with dynamic attention enables multiplexing the feature representation corresponding to multiple hypotheses within a fixed-dimensional feature representation.

Let \mathbf{F}_{sq} , \mathbf{F}_{ex} , \mathbf{F}_{atn} denote the *squeeze*, *excite*, and *attend* operations, respectively, within MHAB. We represent λ as the one hot representation of scalar λ . The feature map \mathbf{X} is transformed to $\mathbf{X}' = [\mathbf{x}'_1, \mathbf{x}'_2, \dots, \mathbf{x}'_C]$ as follows,

$$s_c = \mathbf{F}_{sq}(\mathbf{x}_c), \quad (2)$$

$$\mathbf{e} = \mathbf{F}_{ex}(\mathbf{s}), \quad (3)$$

$$\mathbf{a} = \mathbf{F}_{atn}(\lambda), \quad (4)$$

$$\mathbf{x}'_c = (a_c \times e_c) \mathbf{x}_c, \quad (5)$$

s.t. $\mathbf{s} = [s_1, \dots, s_C]$, $\mathbf{a} = [a_1, \dots, a_C]$ and $\mathbf{e} = [e_1, \dots, e_C]$. \mathbf{F}_{sq} *squeezes* the global spatial information into a channel descriptor using global average pooling. \mathbf{F}_{ex} allows modeling for channel-wise interactions on the output of \mathbf{F}_{sq} . \mathbf{F}_{ex} is implemented as a two layer, fully-connected, neural network. Following the output of the excite block, we modulate the channel-wise activations based on the output of another simple neural network \mathbf{F}_{atn} that takes λ as an input. \mathbf{F}_{atn} has a similar design to \mathbf{F}_{ex} . Please refer to the supplementary material for details.

Figure 2 visualizes the predicted heatmaps from HRNet and MHPNet (using $N = 2$). Note that HRNet only outputs the heatmap corresponding to the foreground person while MHPNet predicts heatmaps for both persons using different values of λ at inference.

4. Experiments

We evaluate MHPNet on three datasets: *Common-Objects in Context*-COCO [22], *CrowdPose* [20] and *Occluded Humans*-OCHuman [43]. These datasets represent varying degrees of occlusion/crowding (see Table 1) and help illustrate the benefits of predicting multiple hypotheses in top-down methods. We report standard metrics such as AP, AP⁵⁰, AP⁷⁵, AP^M, AP^L, AR, AP^{easy}, AP^{med} and AP^{hard} at various Object Keypoint Similarity as defined in [22, 20]. We report results using ground truth bounding boxes as well as bounding boxes obtained via Faster R-CNN [34].

We compare MHPNet against recent state-of-the-art networks, namely, SimpleBaseline [39] and HRNet [36]. When comparing with HRNet, MHPNet employs a similar feature extraction backbone and adds MHAB at the output of the convolutional blocks at the end of stages 3 and 4 [36]. For comparisons with SimpleBaseline [39], two MHABs are added to the last two ResNet blocks in the encoder. Please see the supplementary materials for architecture details. All experiments use $N = 2$, predicting two hypotheses for each input (also see Sect. 5).

Method	Arch	#Params	AP	AP ⁵⁰	AP ⁷⁵	AP ^M	AP ^L	AR
SBL†	R-50	34.0M	72.4	91.5	80.4	69.7	76.5	75.6
MHPNet†	R-50	35.0M (+2.8%)	73.3 (+0.9)	93.3	81.2	70.6	77.6	76.7
SBL†	R-101	53.0M	73.4	92.6	81.4	70.7	77.7	76.5
MHPNet†	R-101	54.0M (+1.7%)	74.1 (+0.7)	93.3	82.3	71.3	78.6	77.4
SBL†	R-152	68.6M	74.3	92.6	82.5	71.6	78.7	77.4
MHPNet†	R-152	69.6M (+1.4%)	74.8 (+0.5)	93.3	82.4	71.7	79.4	78.2
SBL★	R-50	34.0M	74.1	92.6	80.5	70.5	79.6	76.9
MHPNet★	R-50	35.0M (+0.4%)	75.3 (+1.2)	93.4	82.4	72.0	80.4	78.4
SBL★	R-101	35.0M	75.5	92.5	82.6	72.4	80.8	78.4
MHPNet★	R-101	54.0M (+0.3%)	76.0 (+0.5)	93.4	83.5	72.6	81.1	79.1
SBL★	R-152	68.6M	76.6	92.6	83.6	73.7	81.3	79.3
MHPNet★	R-152	69.6M (+2.8%)	77.0 (+0.4)	93.5	84.3	73.7	81.9	80.0
HRNet†	H-32	28.5M	76.5	93.5	83.7	73.9	80.8	79.3
MHPNet†	H-32	28.6M (+1.7%)	77.6 (+1.1)	94.4	85.3	74.7	81.9	80.6
HRNet†	H-48	63.6M	77.1	93.6	84.7	74.1	81.9	79.9
MHPNet†	H-48	63.7M (+1.4%)	77.6 (+0.5)	94.4	85.4	74.6	82.1	80.6
HRNet★	H-32	28.5M	77.7	93.6	84.7	74.8	82.5	80.4
MHPNet★	H-32	28.6M (+0.4%)	78.5 (+0.8)	94.4	85.7	75.6	83.0	81.4
HRNet★	H-48	63.6M	78.1	93.6	84.9	75.3	83.1	80.9
MHPNet★	H-48	63.7M (+0.3%)	78.8 (+0.7)	94.4	85.7	75.5	83.7	81.6

Table 2: MHPNet improves performance on COCO val set across various architectures and input sizes (using ground-truth bounding boxes for evaluation). #Params are reported only for the pose estimation network, excluding bounding box computation. R-@ and H-@ stands for ResNet-@ and HRNet-W@ respectively. † and ★ denotes input resolution of 256×192 and 384×288 respectively. SBL refers to SimpleBaseline [39].

4.1. COCO Dataset

Dataset: COCO contains 64K images and 270K person instances labeled with 17 keypoints. For training we use the train set (57K images, 150K persons) and for evaluation we use the val (5K images, 6.3K persons) and the test-dev set (20K images). The input bounding box is extended in either height or width to obtain a fixed aspect ratio of 4 : 3. The detection box is then cropped from the image and is resized to a fixed size of either 256×192 or 384×288 , depending on the experiment. Following [27], we use data augmentation with random rotation ($[-45^\circ, 45^\circ]$), random scale ($[0.65, 1.35]$), flipping, and half-body crops. Following [28, 36, 39], we use flipping and heatmap offset during inference.

Results: Table 2 compares the performance of MHPNet with SimpleBaseline (denoted as SBL) and HRNet using ground truth bounding boxes. MHPNet outperforms the baseline across various backbones and input sizes. Using ResNet-50 backbone, MHPNet improves the SimpleBaseline results by 0.9 AP for smaller input size and 1.2 AP for larger input size. Comparing with HRNet, MHPNet shows an improvement ranging from 0.7 to 1.1 AP on various architectures and input sizes. Note that MHPNet results in < 3% increase in parameters compared to the baselines.

When using bounding boxes obtained from Faster R-CNN, as expected, MHPNet performs comparably to HRNet (Table 5). Unsurprisingly, since most of the COCO bounding

Arch	AP	AP ⁵⁰	AP ⁷⁵	AP ^{easy}	AP ^{med}	AP ^{hard}
HRNet-W32†	70.0	91.0	76.3	78.8	70.3	61.7
MHPNet†	71.2	91.9	77.4	78.8	71.5	63.8
HRNet-W48†	71.3	91.1	77.5	80.5	71.4	62.5
MHPNet†	72.8	92.0	79.2	80.6	73.1	65.2
HRNet-W32★	71.6	91.1	77.7	80.4	72.1	62.6
MHPNet★	73.0	91.8	79.3	80.7	73.3	65.5
HRNet-W48★	72.8	92.1	78.7	81.3	73.3	64.0
MHPNet★	73.7	91.9	80.0	80.7	74.1	66.5

Table 3: MHPNet outperforms HRNet on CrowdPose val set. † and ★ denote input resolution of 256×192 and 384×288 , respectively.

boxes contain a single person. The benefits of MHPNet are apparent on more challenging CrowdPose and OCHuman datasets (Sect. 4.2, 4.3).

4.2. CrowdPose Dataset

Dataset: CrowdPose contains 20K images and 80K persons labeled with 14 keypoints. CrowdPose has more crowded scenes as compared to COCO, but the index of crowding is less compared to the OCHuman [43]. For training, we use the train set (10K images, 35.4K persons) and for evaluation we use the val set (2K images, 8K persons) and test set (8K images, 29K persons).

Results: Table 3 compares the performance of MHPNet with HRNet when evaluated using ground-truth bounding boxes. MHPNet outperforms HRNet with improvements

in AP ranging from 0.9 to 1.5 across different input sizes. As shown in Table 5, when evaluated using Faster R-CNN bounding boxes, MHPNet outperforms the published state-of-the-art HigherHRNet [7] (bottom-up method, multi-scale testing) model by 2.4 AP on the `test` set. For completeness, we also trained and evaluated HRNet on CrowdPose. MHPNet outperforms HRNet by 0.7 AP on the `test` set and 0.8 AP on the `val` set. We report additional metrics in the supplementary material.

Method	Arch	AP	AP ⁵⁰	AP ⁷⁵	AP ^M	AP ^L	AR
SBL†	R-50	56.3	76.1	61.2	66.4	56.3	61.0
MHPNet†	R-50	64.4 (+8.1)	86.0	70.4	66.8	64.4	72.3
SBL†	R-101	60.5	77.2	66.6	68.3	60.5	64.7
MHPNet†	R-101	68.2 (+7.7)	87.4	75.1	67.0	68.2	75.5
SBL†	R-152	62.4	78.3	68.1	68.3	62.4	66.5
MHPNet†	R-152	70.3 (+7.9)	88.6	77.9	66.9	70.2	77.0
SBL★	R-50	55.8	74.8	60.4	64.7	55.9	60.7
MHPNet★	R-50	66.3 (+10.5)	87.5	72.2	66.0	66.3	74.1
SBL★	R-101	61.6	77.2	66.6	62.1	61.6	65.8
MHPNet★	R-101	70.3 (+8.7)	88.4	77.1	64.1	70.4	77.7
SBL★	R-152	64.2	78.3	69.1	66.5	64.2	68.1
MHPNet★	R-152	72.4 (+8.2)	89.5	79.5	67.7	72.5	79.6
HRNet†	H-32	63.1	79.4	69.0	64.2	63.1	67.3
MHPNet†	H-32	72.5 (+9.4)	89.2	79.4	65.1	72.6	79.1
HRNet†	H-48	64.5	79.4	70.1	65.1	64.5	68.5
MHPNet†	H-48	72.2 (+7.7)	89.5	78.7	66.5	72.3	79.2
HRNet★	H-32	63.7	78.4	69.0	64.3	63.7	67.6
MHPNet★	H-32	72.7 (+9.0)	89.6	79.6	66.5	72.7	79.7
HRNet★	H-48	65.0	78.4	70.3	68.4	65.0	68.8
MHPNet★	H-48	74.1 (+9.1)	89.7	80.1	68.4	74.1	81.0

Table 4: Comparisons on OCHuman `val` set with ground-truth bounding box evaluation after training on COCO `train` set. † and ★ denotes input resolution of 256×192 and 384×288 respectively. R-@ denotes ResNet-@ and H-@ denotes HRNet-W@. SBL refers to SimpleBaseline [39].

4.3. OCHuman Dataset

Dataset: OCHuman is focused on heavily occluded humans. It contains 4731 images and 8110 persons labeled with 17 keypoints. In OCHuman, on an average 67% of the bounding box area has overlap with other bounding boxes [43], compared to only 0.8% for COCO. Additionally, the number of examples with occlusion IoU > 0.5 is 68% for OCHuman, compared to 1% for COCO (Table 1). This makes the OCHuman dataset complex and challenging for human pose estimation under occlusion. The single person assumption made by existing top-down methods is not entirely applicable to examples in this dataset.

Similar to [43], we use the `train` set of COCO for training. Note that we do not train on the OCHuman `train` set. For evaluation, we use the `val` set (2,500 images, 4,313 persons) and the `test` set (2,231 images, 3,819 persons).

Results: Table 4 compares the performance of MHP-

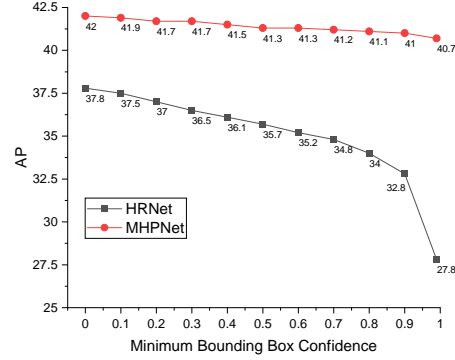


Figure 4: Unlike HRNet, MHPNet maintains a stable performance as a function of detector confidence for selecting input bounding boxes. Results are shown using HRNet-W48- 384×288 evaluated on OCHuman `val` set.

Net with SimpleBaseline and HRNet on OCHuman when evaluated with ground truth bounding boxes on the `val` set. MHPNet significantly outperforms SimpleBaseline with improvements in AP ranging from 7.7 to 10.5, across various architectures and input sizes. Similarly, for HRNet the performance gains between 7.7 to 9.4 AP are observed.

Current state-of-the-art results on OCHuman are reported by HGG [16] (bottom-up method, multi-scale testing) as shown in Table 5. In addition, we also evaluated HRNet using Faster R-CNN bounding boxes on OCHuman for a fair comparison. MHPNet outperforms HRNet and HGG by 5.3 AP and 6.5 AP, respectively, on the `test` set. The improvements are significant and to the best of our knowledge, this is the first time a top-down method has outperformed the state-of-the-art bottom-up method on OCHuman.

Figure 8 shows qualitative results on several examples from OCHuman, highlighting the effectiveness of MHPNet in recovering multiple poses under challenging conditions. In some cases, MHPNet can fail due to large difference in the scale of the various pose instances in a given bounding box, as shown in Figure 7.

Robustness to Human Detector Outputs: The performance of top-down methods is often gated by the quality of human detection outputs. We analyze the robustness of HRNet and MHPNet with varying detector confidence on OCHuman in Fig. 4. As expected, HRNet performance degrades as low confidence bounding boxes are filtered out, leading to missed detections on occluded persons. Specifically, HRNet performance degrades from 37.8 AP (30637 bounding boxes) to 32.8 AP (6644 bounding boxes), when the detector confidence is varied from 0 to 0.9. Since HRNet is only able to provide a single output per bounding box, the average precision drops corresponding to misdetections on the occluded persons. In contrast, MHPNet maintains a relatively stable performance (drop of 1 AP) as shown in Fig. 4 for the same inputs. Since MHPNet can predict

Method	COCO		CrowdPose		OCHuman	
	val	test	val	test	val	test
CrowdPose [20]	-	70.9	-	66.0	-	-
HigherHRNet* [7]	67.1	70.5	-	67.6	-	-
OCHuman [43]	55.2	-	-	-	22.2	23.8
HGG* [16]	68.3	67.6	-	-	41.8	36.0
HRNet [36]	76.3	75.5	<i>68.0</i>	<i>69.3</i>	<i>37.8</i>	<i>37.2</i>
MHPNet (Ours)	76.3	75.3	68.8	70.0	42.0	42.5

Table 5: Comparison with state-of-the-art methods using bounding boxes from a human detector on various datasets. * denotes bottom-up methods. The numbers in *italics* are our evaluation of HRNet on these datasets. Other numbers are reported from the respective publications.

Pose Enhancement	HRNet	MHPNet
DARK [42]	78.8	79.4
PoseFix [26]	79.5	79.9
DARK-PoseFix	79.5	80.0

Table 6: Improvement in MHPNet performance on COCO val set using various pose enhancement methods.

multiple hypotheses, it can recover pose configurations for occluded persons despite misdetection of their corresponding bounding boxes. This is a desirable property afforded by our proposed multi-hypothesis attention network.

5. Discussions

Number of Hypothesis N : By design, MHPNet supports predicting any number of hypotheses, N , at the expense of linearly increasing the inference time with N . Trivially, $N = 1$ without MHAB is equivalent to baseline top-down methods. Section 4 have shown improvements in performance using $N = 2$ for MHPNet. However, we did not observe any further improvements using $N = 3$. This is consistent with the fact that most datasets have few examples with three or more ground-truth pose instances per bounding box (Fig. 6).

Improvements to MHPNet: As shown in Table. 6, pose enhancement methods such as DARK [42] and PoseFix [26] can further improve the performance of MHPNet.

Visualization with continuous λ : MHPNet’s ability to predict multiple hypotheses provides a useful tool to visualize how attention can dynamically switch between various pose configurations during inference. Fig. 5 shows how the predicted keypoints gradually shift from the foreground person to the other pose instance within the bounding box, as λ is varied from 0 to 1.

6. Conclusion

Top-down 2D pose estimation methods make the key assumption of a single person within the input bounding box

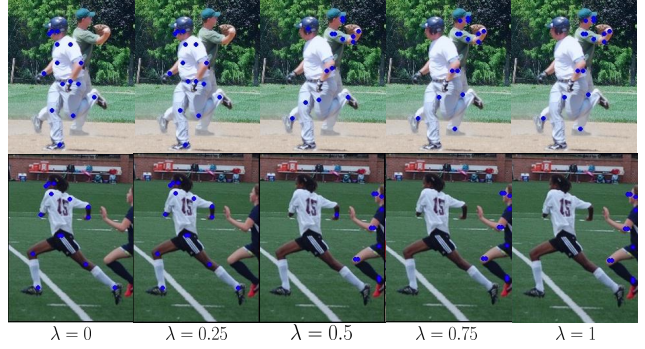


Figure 5: As λ is varied from 0 to 1 during inference, the key-points (in blue) gradually shift from the foreground person to the other pose instance within the bounding box.

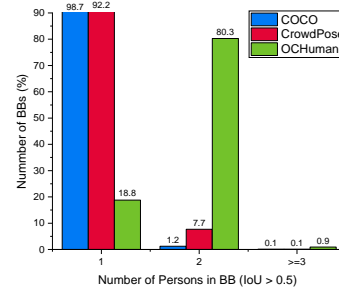


Figure 6: Percentage of examples with 1, 2 and 3+ pose instances per ground truth bounding box in various datasets.



Figure 7: MHPNet fails in some cases with significant scale difference between multiple persons in the bounding box.

during training and inference. While these methods have shown impressive results, the single person assumption limits their ability to perform well in crowded scenes with occlusions. Our proposed Multi-Hypothesis Attention Network, MHPNet, enables top-down methods to predict multiple hypotheses for a given input. Our approach is efficient in terms of the number of additional network parameters and is stable with respect to the quality of the input bounding boxes. MHPNet achieves state-of-art results on challenging datasets with significant crowding and occlusions. We believe that the concept of predicting multiple hypotheses is an important conceptual change and will inspire a new research direction for top-down methods.

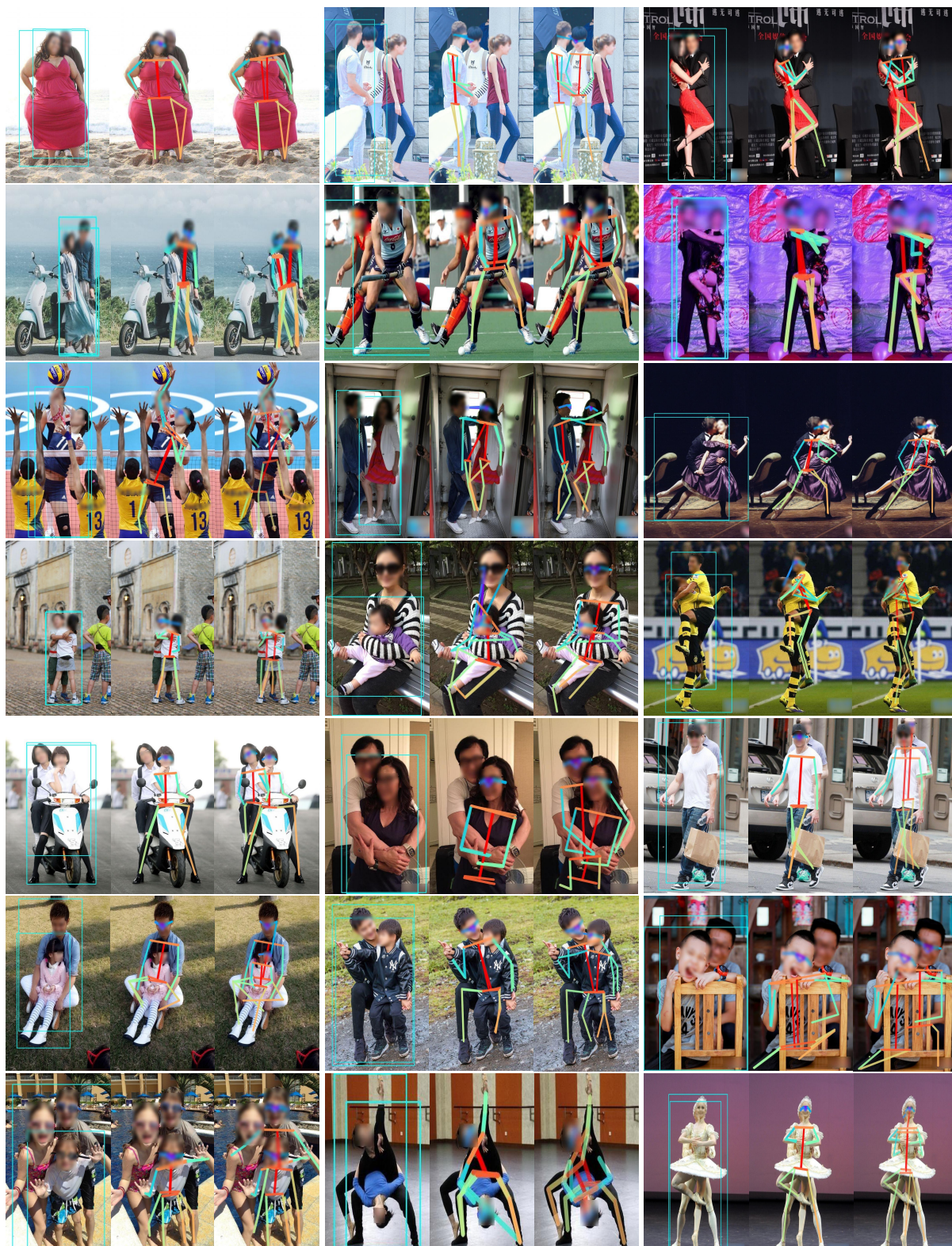


Figure 8: Qualitative results on OCHuman val set. Each image (left to right) shows input bounding boxes, HRNet predictions and MHPNet predictions. Due to occlusions, HRNet often misses the person in the background which is recovered by MHPNet. Please see additional results in supplementary materials.

7. Appendix

7.1. MHAB Code

In this section, we describe the code of MHAB in PyTorch. The code in Listing. 1 outlines the details of functions F_{sq} , F_{ex} and F_{atn} . F_{sq} is a simple global average pool and F_{ex} and F_{atn} are two-layered neural networks. MHAB can be incorporated in any existing feature extraction backbone, with a relatively simple (< 15 lines) code change.

```

1 class MHAB(nn.Module):
2     def __init__(self, num_channels=c, reduce=r):
3         super(MHAB, self).__init__()
4         self.F_sqn = nn.AdaptiveAvgPool2d(1)
5
6         self.F_ex = nn.Sequential(
7             nn.Linear(c, c // r, bias=False),
8             nn.ReLU(inplace=True),
9             nn.Linear(c // r, c, bias=False),
10            nn.Sigmoid()
11        )
12
13        self.F_atn = nn.Sequential(
14            nn.Linear(2, c // r),
15            nn.BatchNorm1d(c // r),
16            nn.ReLU(inplace=True),
17            nn.Linear(c // r, c),
18            nn.Sigmoid()
19        )
20
21        return
22
23    def forward(self, x, lambda):
24        b, c, _, _ = x.size()
25        y = self.F_sqn(x).view(b, c)
26        y = self.F_ex(y).view(b, c, 1, 1)
27
28        z = self.F_atn(lambda).view(b, c, 1, 1)
29
30        out = x * y.expand_as(x) * z.expand_as(x)
31        return out

```

Listing 1: Code for MHAB.

7.2. Architecture Details

MHPNet-HRNet: Figure. 9 shows the architecture details of HRNet [36]. For simplicity, we only show backbone HRNet-W32 at input size 256×192 , other HRNet backbones follow similar pipeline. Figure. 10 shows the architecture of MHPNet, where multiple MHABs are inserted at various stages.

MHPNet-SimpleBaseline: Figure. 11 shows the architecture details of SimpleBaseline [39]. Figure. 12 shows the architecture of MHPNet, where multiple MHABs are inserted in the encoder of the pose estimator..

7.3. Robustness to Bounding Box Confidence

Table 7 illustrates the number of Faster-RCNN bounding boxes as a function of minimum bounding box confidence. Notice that a majority of all available bounding boxes (min. confidence = 0.0) have confidence < 0.4 .

Min. BB Confid.	OCHuman	
	val	test
0.0	30637	26992
0.1	22247	19704
0.2	16273	14613
0.3	13603	12216
0.4	11944	10767
0.5	10654	9645
0.6	9626	8697
0.7	8699	7880
0.8	7768	7018
0.9	6644	5989
0.99	4416	3883

Table 7: Number of Faster-RCNN bounding boxes greater than a given confidence score.

Inference	COCO	CrowdPose	OCHuman
HRNet	78.1	72.8	65.0
MHPNet (SHP, $\lambda = 1$)	55.8	42.2	41.4
MHPNet (SHP, $\lambda = 0$)	78.3	72.7	65.7
MHPNet (MHP)	78.8	73.7	74.1

Table 8: Performance of each individual hypothesis of MHPNet on val sets using ground truth bounding boxes. We use the backbone W48 with image resolution 384×288 , and compare with the same HRNet configuration. By default, HRNet only predicts a single hypothesis.

We compare the performance of MHPNet to HRNet as a function of varying minimum confidence on OCHuman test dataset in Fig. 14 and val dataset in Fig. 13 (also shown in the paper). MHPNet is much more stable w.r.t bounding box confidence thresholding, as compared to baseline networks like HRNet. We note that while MHPNet AP drops from 42.5 to 41.4 (1.1 AP drop) on test set at minimum confidence of 0.9, HRNet drops by more than 6 AP. This performance is consistent with the performance on the val dataset (Fig. 4 in the paper).

7.4. Individual Hypothesis Performance

It is interesting to compare the performance of each individual hypothesis predicted by MHPNet in isolation. Since $\lambda = 0$ correspond to the primary hypothesis (centered on the person), only using the primary hypothesis for inference is expected to give better results compared to only using $\lambda = 1$ hypothesis during inference. In addition, we also expect $\lambda = 0$ hypothesis to provide similar performance as baseline top-down network, if used in isolation. Table 8 shows the performance of each individual hypothesis mode of MHPNet with HRNet-W48 backbone at input size 384×288 on various datasets, using ground truth bounding boxes. Note that when using only a single hypothesis from MHPNet for

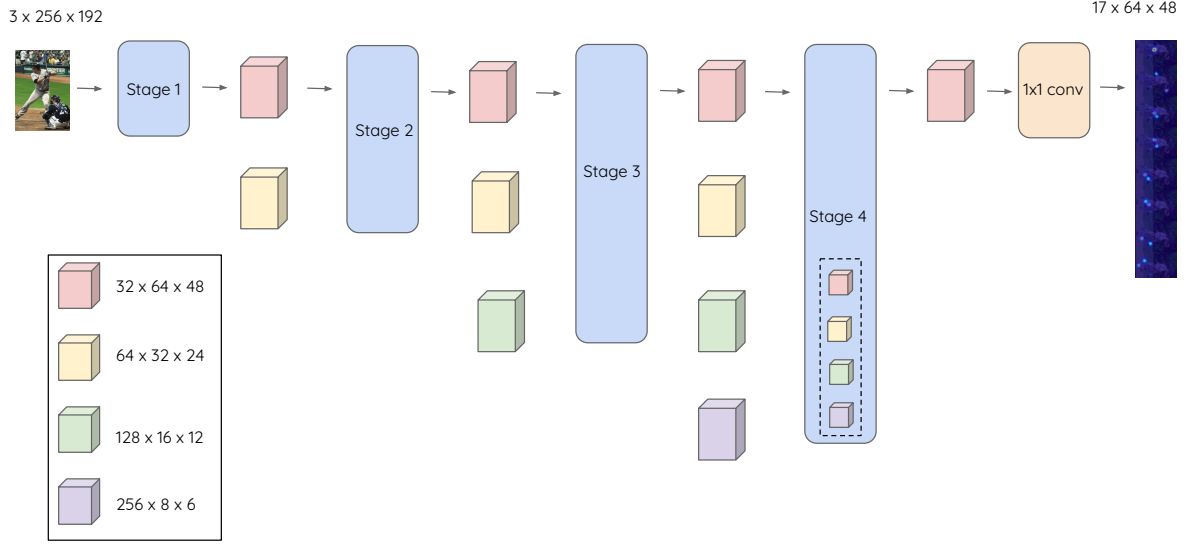


Figure 9: Illustration of HRNet-W32 backbone at input resolution 256×192 . The blue blocks depict the four stages in the architecture.

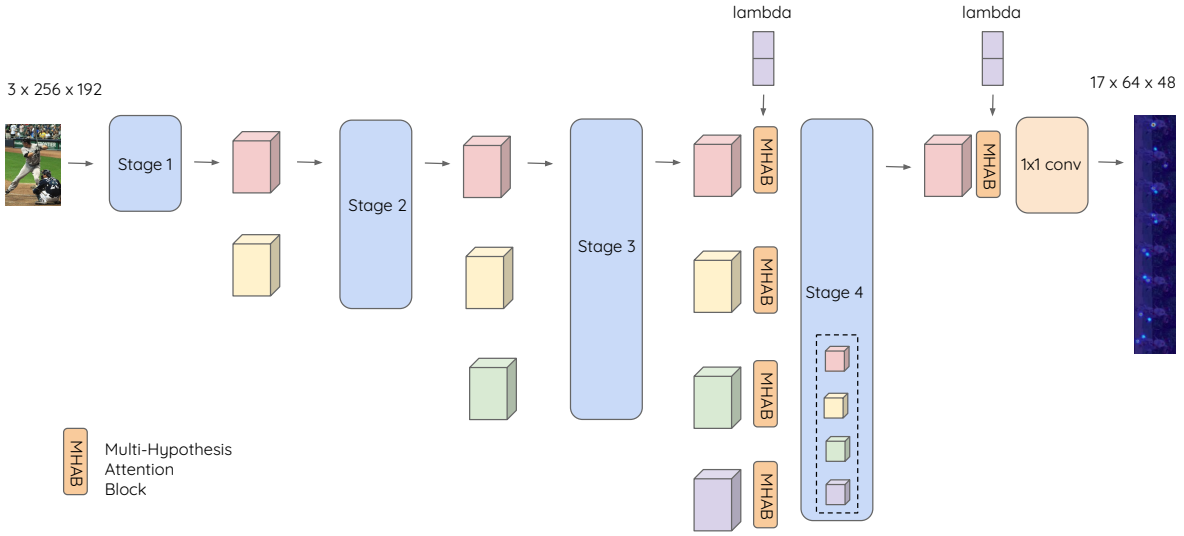


Figure 10: Illustration of MHPNet with HRNet-W32 backbone at input resolution 256×192 . We insert 5 MHABs into the HRNet, 4 MHABs after Stage 3 and 1 MHAB after Stage 4.

inference, performance of primary hypothesis ($\lambda = 0$) is similar to HRNet. When using multiple hypothesis during inference, we get an improvement of 8.4 AP (65.7 to 74.1 AP) on the OCHuman dataset.

7.5. Ablation: MHAB

In this section, we study the effect of ablation for MHAB. As outlined in the paper, MHAB consists of three operations *squeeze* \mathbf{F}_{sq} , *excite* \mathbf{F}_{ex} and *attend* \mathbf{F}_{atn} . Of the three operations, the *attend* operation \mathbf{F}_{atn} consumes the λ pa-

rameter that we pass as additional input to MHAB. In Tab. 9, we show the effect of only using the attention block by disabling \mathbf{F}_{sq} and \mathbf{F}_{ex} , in the first row for both COCO and OCHuman val datasets. Note that these numbers are lower than corresponding experiments that use \mathbf{F}_{sq} and \mathbf{F}_{ex} operations, by 0.3 AP for COCO (Tab. 2, last row in paper) and 3.3 AP (Tab. 4, last row in paper) for OCHuman val datasets. This confirms that all three operations contribute to MHAB, and therefore to MHPNet. We further study the effect of varying the intermediate linear layer within \mathbf{F}_{sq} and

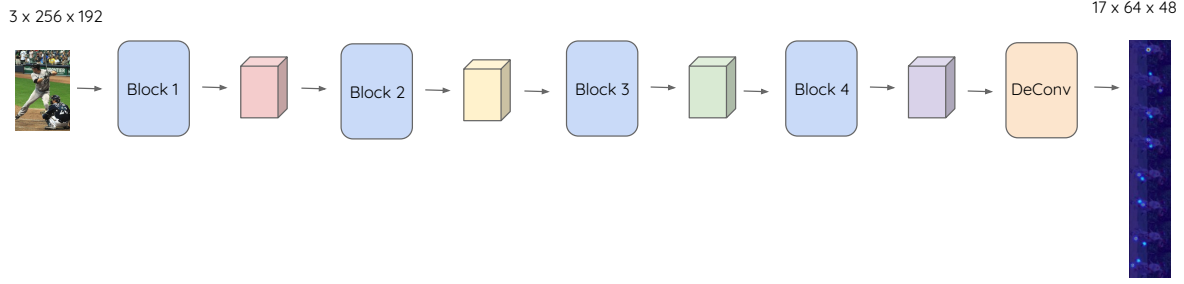


Figure 11: Illustration of SimpleBaseline architecture. The blue blocks represent the four blocks in the encoder of SimpleBaseline.

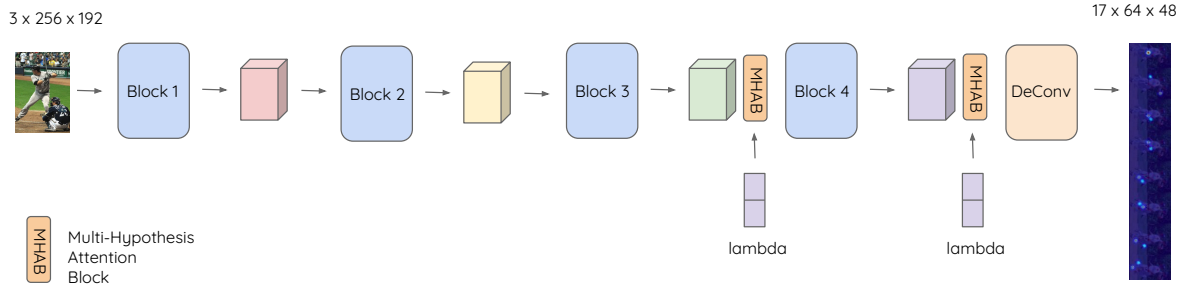


Figure 12: Illustration of MHPNet with SimpleBaseline architecture. We insert 2 MHABs into the encoder after Block 3 and Block 4.

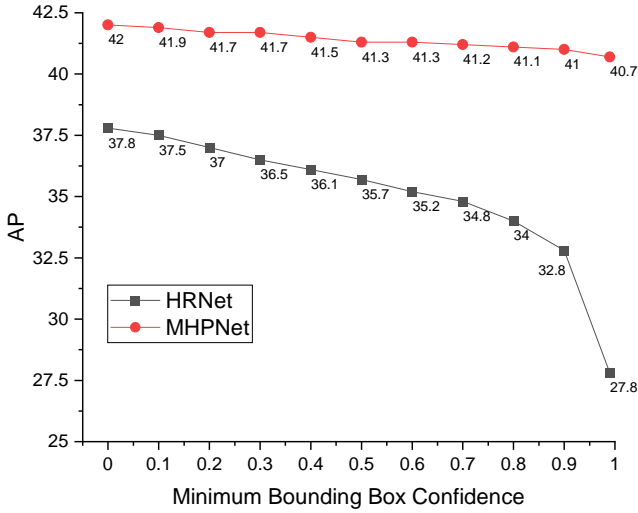


Figure 13: Unlike HRNet, MHPNet maintains a stable performance as a function of detector confidence for selecting input bounding boxes. Results are shown using HRNet-W48-384 x 288 evaluated on the val set of OCHuman.

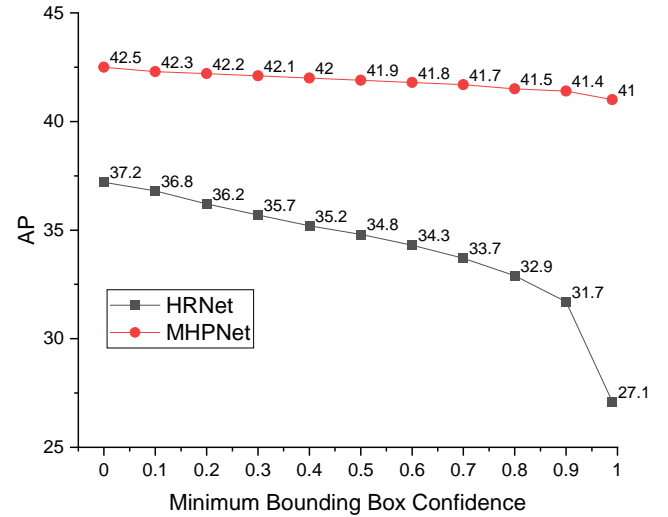


Figure 14: Similar to Figure 13 we show results on the test set of OCHuman.

7.6. Qualitative Results

Figure 15 and Figure 16 shows additional results on the OCHuman dataset, comparing MHPNet to HRNet. Note that in all of these cases, HRNet faces the problem of having highly overlapping bounding boxes because of the spatial

F_{ex} , which is controlled by the `reduce` parameter [12] in Listing 1. While all the results reported in the paper use the default value of `reduce=4`, we show that `reduce=2` and `reduce=1` show comparable results.

Method	Arch	Ablation	AP	AP ⁵⁰	AP ⁷⁵	AP ^M	AP ^L	AR	AR ⁵⁰	AR ⁷⁵	AR ^M	AR ^L
			COCO									
MHPNet	H-48	only attention	78.5	94.4	85.5	75.3	83.5	81.4	95.8	87.5	77.8	86.7
MHPNet	H-48	reduce=1	78.8	94.4	85.8	75.5	83.6	81.5	95.4	87.8	78.0	86.6
MHPNet	H-48	reduce=2	78.8	94.4	85.6	75.8	83.6	81.7	95.7	87.7	78.3	86.8
MHPNet	H-48	reduce=4	78.8	94.4	85.7	75.5	83.7	81.6	95.5	87.5	78.0	86.8
			OCHuman									
MHPNet	H-48	only attention	70.8	89.8	77.5	65.7	70.9	77.9	94.2	84.2	68.6	77.9
MHPNet	H-48	reduce=1	74.4	90.7	80.9	66.9	74.4	81.2	95.1	87.2	70.0	81.2
MHPNet	H-48	reduce=2	74.0	90.1	80.3	63.6	74.0	80.7	94.5	86.7	68.6	80.7
MHPNet	H-48	reduce=4	74.1	89.7	80.1	68.4	74.1	81.0	94.4	87.0	72.9	81.0

Table 9: We illustrate different ablations of MHAB. For MHPNet with backbone W48 on resolution 384×288 , we train models with varying capacity for *squeeze* \mathbf{F}_{sq} and *excite* \mathbf{F}_{ex} operations. When both operations are disabled, and only *attention* operation \mathbf{F}_{atn} is used within MHAB, we get sub-optimal results on both COCO _{val} (0.3 AP drop) and OCHuman _{val} (3.6 AP drop) datasets (first row of each dataset). When *squeeze* and *excite* operations are employed, we get a good performance boost, especially on the OCHuman _{val} dataset. All results in the paper employ `reduce=4` (bold).

proximity of humans in these images. Consequently, HR-Net picks one dominant person and detects key-points on the same person within both bounding box instances. In contrast, MHPNet can clearly identify the correct set of key-points and associate them to the correct human(s) in each example. We especially want to point attention to the cases where people are dancing in tandem, or tackling each other while playing sports. Such situations produce extremely complicated occlusions. However, MHPNet is able to successfully attribute the correct key-points to each human in the input bounding boxes in such situations, highlighting its usefulness in occlusion scenarios.

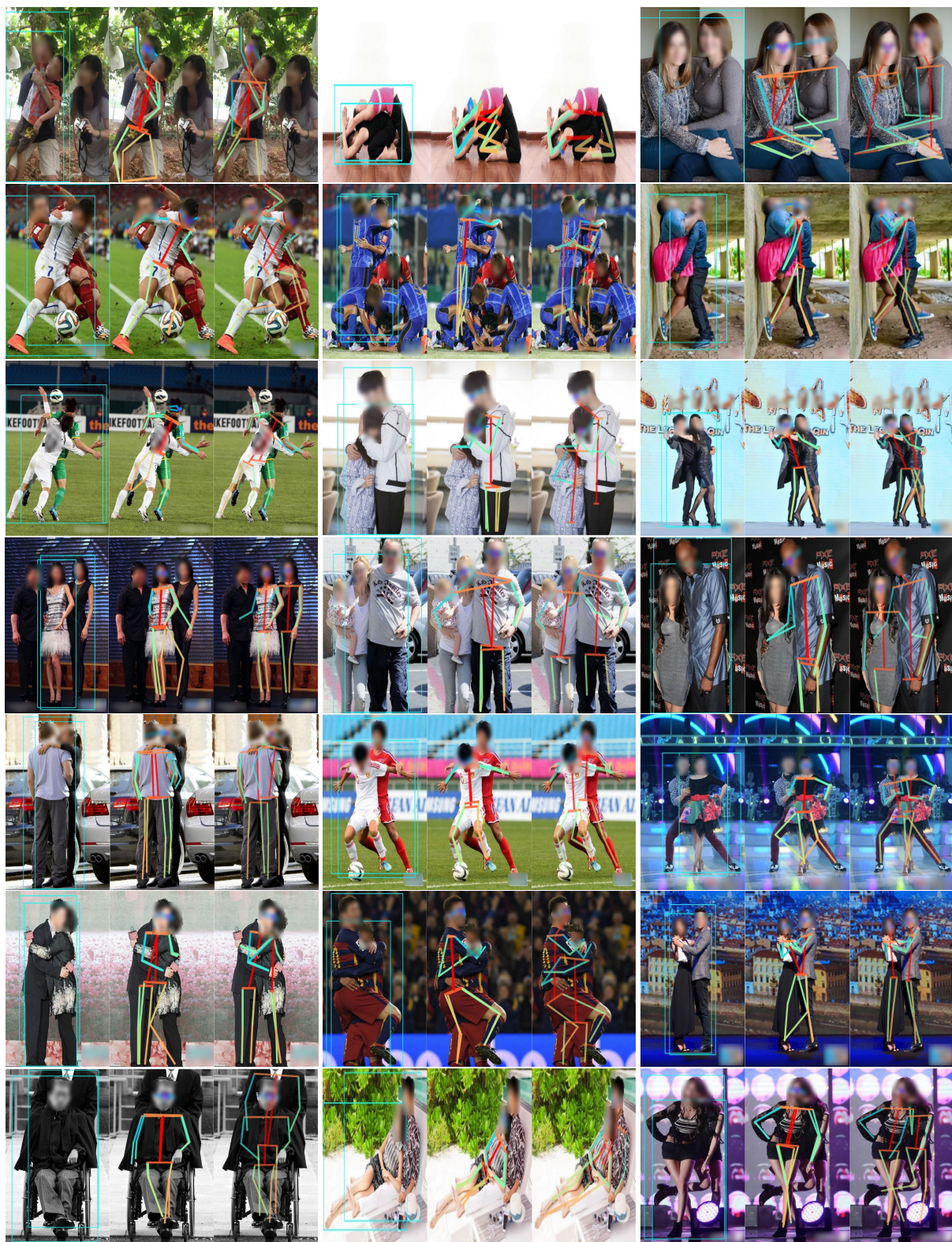


Figure 15: Qualitative results of MHPNet. Each image (left to right) shows input bounding boxes, HRNet predictions and MHPNet predictions.

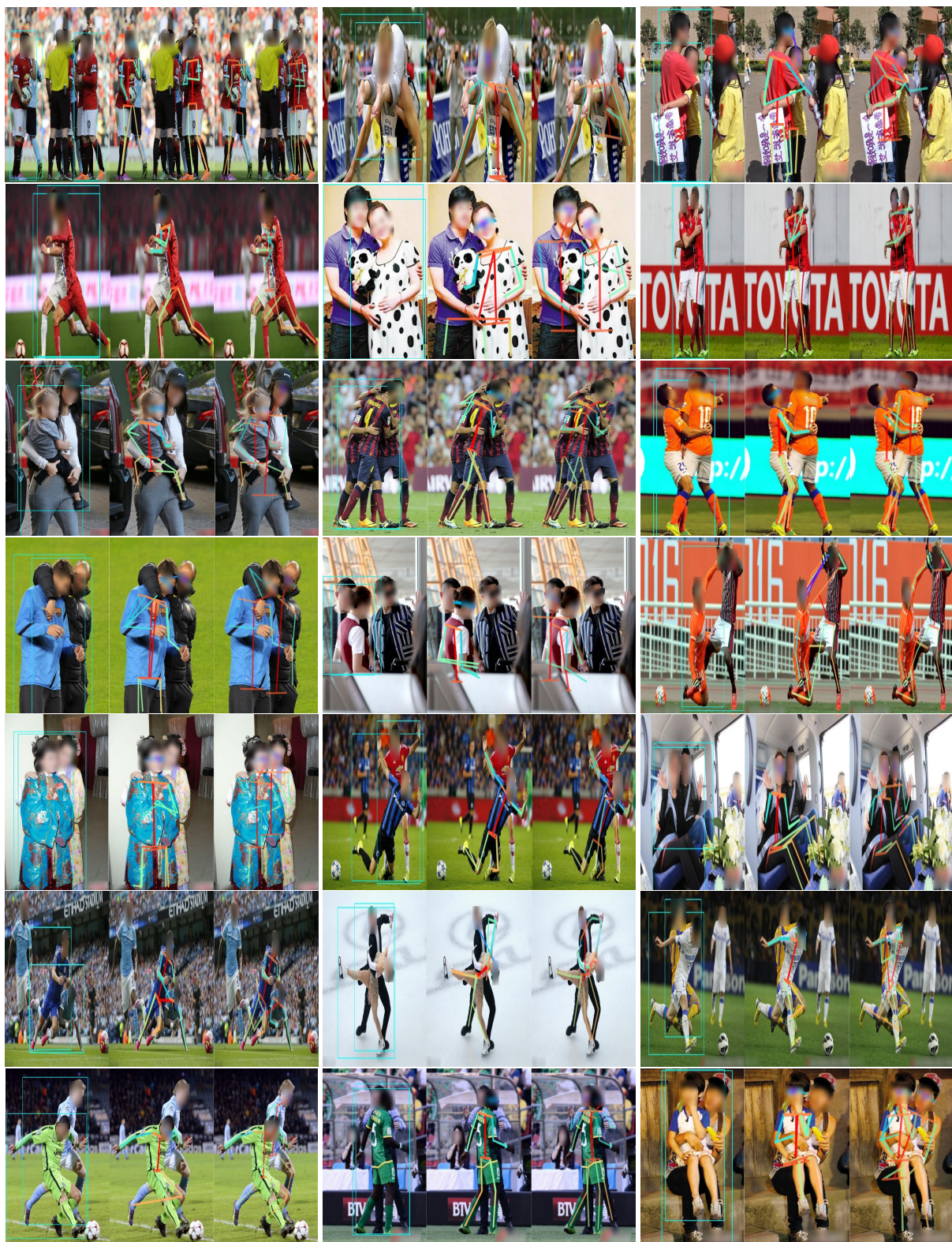


Figure 16: Qualitative results of MHPNet.

References

- [1] Mykhaylo Andriluka, Umar Iqbal, Eldar Insafutdinov, Leonid Pishchulin, Anton Milan, Juergen Gall, and Bernt Schiele. Posetrack: A benchmark for human pose estimation and tracking. In *Proceedings of the IEEE Conference on Computer Vision and Pattern Recognition*, pages 5167–5176, 2018. 2
- [2] Mykhaylo Andriluka, Leonid Pishchulin, Peter Gehler, and Bernt Schiele. 2d human pose estimation: New benchmark and state of the art analysis. In *IEEE Conference on Computer Vision and Pattern Recognition (CVPR)*, June 2014. 2
- [3] Z Cao, T Simon, S Wei, and Y Sheikh. Realtime multi-person 2d pose estimation using part affinity fields. corr abs/1611.08050. *arXiv preprint arXiv:1611.08050*, 2016. 1, 3
- [4] Rich Caruana. Multitask learning. *Machine learning*, 28(1):41–75, 1997. 3
- [5] Yilun Chen, Zhicheng Wang, Yuxiang Peng, Zhiqiang Zhang, Gang Yu, and Jian Sun. Cascaded pyramid network for multi-person pose estimation. In *Proceedings of the IEEE conference on computer vision and pattern recognition*, pages 7103–7112, 2018. 1, 3
- [6] Bowen Cheng, Yunchao Wei, Honghui Shi, Rogerio Feris, Jinjun Xiong, and Thomas Huang. Revisiting rcnn: On awakening the classification power of faster rcnn. In *Proceedings of the European conference on computer vision (ECCV)*, pages 453–468, 2018. 3
- [7] Bowen Cheng, Bin Xiao, Jingdong Wang, Honghui Shi, Thomas S Huang, and Lei Zhang. Higherhrnet: Scale-aware representation learning for bottom-up human pose estimation. *arXiv preprint arXiv:1908.10357*, 2019. 2, 3, 6, 7
- [8] Alexey Dosovitskiy and Josip Djolonga. You only train once: Loss-conditional training of deep networks. In *International Conference on Learning Representations*, 2019. 3
- [9] Hao-Shu Fang, Shuqin Xie, Yu-Wing Tai, and Cewu Lu. Rmpe: Regional multi-person pose estimation. In *Proceedings of the IEEE International Conference on Computer Vision*, pages 2334–2343, 2017. 3
- [10] Rıza Alp Güler, Natalia Neverova, and Iasonas Kokkinos. Densepose: Dense human pose estimation in the wild. In *Proceedings of the IEEE Conference on Computer Vision and Pattern Recognition*, pages 7297–7306, 2018. 2
- [11] Kaiming He, Georgia Gkioxari, Piotr Dollár, and Ross B Girshick. Mask r-cnn. corr abs/1703.06870 (2017). *arXiv preprint arXiv:1703.06870*, 2017. 1, 3
- [12] Jie Hu, Li Shen, and Gang Sun. Squeeze-and-excitation networks. In *Proceedings of the IEEE conference on computer vision and pattern recognition*, pages 7132–7141, 2018. 4, 11
- [13] Shaoli Huang, Mingming Gong, and Dacheng Tao. A coarse-fine network for keypoint localization. In *Proceedings of the IEEE International Conference on Computer Vision*, pages 3028–3037, 2017. 1, 3
- [14] Eldar Insafutdinov, Leonid Pishchulin, Bjoern Andres, Mykhaylo Andriluka, and Bernt Schiele. Deeppercut: A deeper, stronger, and faster multi-person pose estimation model. In *European Conference on Computer Vision*, pages 34–50. Springer, 2016. 3
- [15] Umar Iqbal and Juergen Gall. Multi-person pose estimation with local joint-to-person associations. In *European Conference on Computer Vision*, pages 627–642. Springer, 2016. 3
- [16] Sheng Jin, Wentao Liu, Enze Xie, Wenhai Wang, Chen Qian, Wanli Ouyang, and Ping Luo. Differentiable hierarchical graph grouping for multi-person pose estimation. In *European Conference on Computer Vision*, pages 718–734. Springer, 2020. 6, 7
- [17] Hanbyul Joo, Hao Liu, Lei Tan, Lin Gui, Bart Nabbe, Iain Matthews, Takeo Kanade, Shohei Nobuhara, and Yaser Sheikh. Panoptic studio: A massively multiview system for social motion capture. In *Proceedings of the IEEE International Conference on Computer Vision*, pages 3334–3342, 2015. 2
- [18] Iasonas Kokkinos. Ubertnet: Training a universal convolutional neural network for low-, mid-, and high-level vision using diverse datasets and limited memory. In *Proceedings of the IEEE Conference on Computer Vision and Pattern Recognition*, pages 6129–6138, 2017. 3
- [19] Sven Kreiss, Lorenzo Bertoni, and Alexandre Alahi. Pifpaf: Composite fields for human pose estimation. In *Proceedings of the IEEE Conference on Computer Vision and Pattern Recognition*, pages 11977–11986, 2019. 1
- [20] Jiefeng Li, Can Wang, Hao Zhu, Yihuan Mao, Hao-Shu Fang, and Cewu Lu. Crowdpose: Efficient crowded scenes pose estimation and a new benchmark. In *Proceedings of the IEEE Conference on Computer Vision and Pattern Recognition*, pages 10863–10872, 2019. 1, 2, 3, 4, 7
- [21] Tsung-Yi Lin, Piotr Dollár, Ross Girshick, Kaiming He, Bharath Hariharan, and Serge Belongie. Feature pyramid networks for object detection. In *Proceedings of the IEEE conference on computer vision and pattern recognition*, pages 2117–2125, 2017. 3
- [22] Tsung-Yi Lin, Michael Maire, Serge Belongie, James Hays, Pietro Perona, Deva Ramanan, Piotr Dollár, and C Lawrence Zitnick. Microsoft coco: Common objects in context. In *European conference on computer vision*, pages 740–755. Springer, 2014. 1, 2, 4
- [23] Wei Liu, Dragomir Anguelov, Dumitru Erhan, Christian Szegedy, Scott Reed, Cheng-Yang Fu, and Alexander C Berg. Ssd: Single shot multibox detector. In *European conference on computer vision*, pages 21–37. Springer, 2016. 3
- [24] Kevis-Kokitsi Maninis, Ilija Radosavovic, and Iasonas Kokkinos. Attentive single-tasking of multiple tasks. In *Proceedings of the IEEE Conference on Computer Vision and Pattern Recognition*, pages 1851–1860, 2019. 3
- [25] Mehdi Mirza and Simon Osindero. Conditional generative adversarial nets. *arXiv preprint arXiv:1411.1784*, 2014. 3
- [26] Gyeongsik Moon, Ju Yong Chang, and Kyoung Mu Lee. Posefix: Model-agnostic general human pose refinement network. In *Proceedings of the IEEE Conference on Computer Vision and Pattern Recognition*, pages 7773–7781, 2019. 7
- [27] Alejandro Newell, Zhiao Huang, and Jia Deng. Associative embedding: End-to-end learning for joint detection and grouping. In *Advances in neural information processing systems*, pages 2277–2287, 2017. 1, 3, 5

- [28] Alejandro Newell, Kaiyu Yang, and Jia Deng. Stacked hour-glass networks for human pose estimation. In *European conference on computer vision*, pages 483–499. Springer, 2016. 1, 3, 5
- [29] George Papandreou, Tyler Zhu, Liang-Chieh Chen, Spyros Gidaris, Jonathan Tompson, and Kevin Murphy. Personlab: Person pose estimation and instance segmentation with a bottom-up, part-based, geometric embedding model. In *Proceedings of the European Conference on Computer Vision (ECCV)*, pages 269–286, 2018. 1
- [30] George Papandreou, Tyler Zhu, Nori Kanazawa, Alexander Toshev, Jonathan Tompson, Chris Bregler, and Kevin Murphy. Towards accurate multi-person pose estimation in the wild. In *Proceedings of the IEEE Conference on Computer Vision and Pattern Recognition*, pages 4903–4911, 2017. 1, 3
- [31] L Pishchulin, E Insafutdinov, S Tang, B Andres, M Andriluka, P Gehler, and Bb Schiele. Deepcut: Joint subset partition and labeling for multi person pose estimation.[arxiv], 2015. 3
- [32] Lingteng Qiu, Xuanye Zhang, Yanran Li, Guanbin Li, Xiaojun Wu, Zixiang Xiong, Xiaoguang Han, and Shuguang Cui. Peeking into occluded joints: A novel framework for crowd pose estimation. *arXiv preprint arXiv:2003.10506*, 2020. 2
- [33] Joseph Redmon and Ali Farhadi. Yolov3: An incremental improvement. *arXiv preprint arXiv:1804.02767*, 2018. 3
- [34] Shaoqing Ren, Kaiming He, Ross Girshick, and Jian Sun. Faster r-cnn: Towards real-time object detection with region proposal networks. In *Advances in neural information processing systems*, pages 91–99, 2015. 2, 3, 4
- [35] Matteo Ruggero Ronchi and Pietro Perona. Supplementary materials for the iccv 2017 paper: Benchmarking and error diagnosis in multi-instance pose estimation. 3
- [36] Ke Sun, Bin Xiao, Dong Liu, and Jingdong Wang. Deep high-resolution representation learning for human pose estimation. In *Proceedings of the IEEE conference on computer vision and pattern recognition*, pages 5693–5703, 2019. 1, 2, 3, 4, 5, 7, 9
- [37] Xiao Sun, Jiaxiang Shang, Shuang Liang, and Yichen Wei. Compositional human pose regression. In *Proceedings of the IEEE International Conference on Computer Vision*, pages 2602–2611, 2017. 1
- [38] Jingdong Wang, Ke Sun, Tianheng Cheng, Borui Jiang, Chaorui Deng, Yang Zhao, Dong Liu, Yadong Mu, Mingkui Tan, Xinggang Wang, et al. Deep high-resolution representation learning for visual recognition. *IEEE transactions on pattern analysis and machine intelligence*, 2020. 1
- [39] Bin Xiao, Haiping Wu, and Yichen Wei. Simple baselines for human pose estimation and tracking. In *Proceedings of the European conference on computer vision (ECCV)*, pages 466–481, 2018. 1, 2, 3, 4, 5, 6, 9
- [40] Makoto Yamada, Leonid Sigal, and Michalis Raptis. No bias left behind: Covariate shift adaptation for discriminative 3d pose estimation. In *European Conference on Computer Vision*, pages 674–687. Springer, 2012. 3
- [41] Amir R Zamir, Alexander Sax, William Shen, Leonidas J Guibas, Jitendra Malik, and Silvio Savarese. Taskonomy: Disentangling task transfer learning. In *Proceedings of the IEEE conference on computer vision and pattern recognition*, pages 3712–3722, 2018. 3
- [42] Feng Zhang, Xiatian Zhu, Hanbin Dai, Mao Ye, and Ce Zhu. Distribution-aware coordinate representation for human pose estimation. In *Proceedings of the IEEE/CVF Conference on Computer Vision and Pattern Recognition*, pages 7093–7102, 2020. 7
- [43] Song-Hai Zhang, Ruilong Li, Xin Dong, Paul Rosin, Zixi Cai, Xi Han, Dingcheng Yang, Haozhi Huang, and Shi-Min Hu. Pose2seg: Detection free human instance segmentation. In *Proceedings of the IEEE conference on computer vision and pattern recognition*, pages 889–898, 2019. 1, 2, 3, 4, 5, 6, 7